JOURNAL OF GEOPHYSICAL RESEARCH, VOL. 115, C08026, doi:10.1029/2009JC005869, 2010

Model-based estimate of the heat budget in the East China Sea

Na Liu,[1,2] Carsten Eden,[3] Heiner Dietze,[3] Dexing Wu,[1] and Xiaopei Lin[1]

Received 2 October 2009; revised 12 February 2010; accepted 8 April 2010; published 25 August 2010.

[1] Using a global ocean model with regionally focused high resolution (1/10°) in the East China Sea (ECS), we studied the oceanic heat budget in the ECS. The modeled sea surface height variability and eddy kinetic energy are consistent with those derived from satellite altimetry. Significant levels of eddy kinetic energy are found east of the Ryukyu Islands and east of Taiwan, where the short-term variability is spawned by active mesoscale eddies coalescing with the circulation. Furthermore, the simulated vertical cross-stream structure of the Kuroshio (along the Pollution Nagasaki line) and the volume transport through each channel in the ECS are in good agreement with the observational estimates. The time-averaged temperature fluxes across the Taiwan Strait (TWS), Tsushima Strait (TSS), and the 200 m isobath between Taiwan and Japan are 0.20 PW, 0.21 PW, and 0.05 PW, respectively. The residual heat flux of 0.04 PW into the ECS is balanced by the surface heat loss. The eddy temperature flux across the 200 m isobath is 0.005 PW, which accounts for 11.2% of the total temperature flux. The Kuroshio onshore temperature flux has two major sources: the Kuroshio intrusion northeast of Taiwan and southwest of Kyushu. The Ekman temperature flux induced by the wind stress in the ECS shows the same seasonal cycle and amplitude as the onshore temperature flux, with a maximum in autumn and a minimum in summer. We conclude that the Ekman temperature flux dominates the seasonal cycle of Kuroshio onshore flux.

Citation: Liu, N., C. Eden, H. Dietze, D. Wu, and X. Lin (2010), Model-based estimate of the heat budget in the East China Sea, *J. Geophys. Res.*, *115*, C08026, doi:10.1029/2009JC005869.

1. Introduction

[2] The East China Sea (ECS) is a marginal sea adjacent to a vast continental shelf toward the western Pacific. Cold, fresh shelf water is distributed on the continental shelf, and warm saline Kuroshio water occupies the area around the shelf break (here defined as the 200 m isobath) and further offshore. The shelf break is a key region influencing the water properties on the shelf as there important onshore cross-frontal transports of heat and freshwater from the Kuroshio take place. Because of their magnitude, these onshore transports are the main agents determining the water mass characteristics of the ECS and its seasonal to interannual variability. Furthermore, the exchange of materials and energy between the Kuroshio and the ECS shapes the biotic environment of the ECS as, e.g., nutrients originating from the Kuroshio may well impinge on primary production on the shelf [*Matsuno et al.*, 2009].

[3] The onshore cross-frontal volume transport has been estimated by several studies [*Guo et al.*, 2006; *Lee and Matsuno*, 2007; *Isobe and Beardsley*, 2006; *Isobe*, 2008]. Using acoustic Doppler current profiler (ADCP) observations in the Taiwan Strait (TWS) and Tsushima Strait (TSS), *Isobe* [2008] estimated the onshore Kuroshio intrusion across the ECS shelf break to be 1.4 Sv. A global ocean model is used by *Fang et al.* [2003] to estimate the volume, heat, and salt transport in the ECS, and the Kuroshio onshore transport is estimated to be 2.2 Sv. The annually averaged onshore transport is estimated to be 1.46 Sv by *Guo et al.* [2006] on the basis of numerical modeling. The mean values of the Taiwan Warm Current and the Tsushima Warm Current are estimated to be 1.60 Sv [*Zhao and Fang*, 1991] and 2.40 Sv [*Isobe et al.*, 2002], respectively, on basis of observations. Note that the onshore cross-frontal transport is comparable with the volume transport of ocean currents over the shelf.

[4] The saline and warm water from the Kuroshio help to maintain the salinity and temperature characteristic for the shelf water in the ECS. With respect to the heat budget in this area, the onshore transport from the Kuroshio might be a major source of heat to the ECS shelf. In this study, our major concern was to quantify the onshore net temperature flux from the Kuroshio into the ECS. We used a global numerical model approach in which the Kuroshio front was reproduced accurately. The numerical model in this study was also required to simulate the large-scale ocean circulation realistically; otherwise, a false structure of the Kuroshio results in frontal characteristics different from those

[1] Physical Oceanography Laboratory, Ocean University of China, Qingdao, China.
[2] Also at Leibniz-Institut für Meereswissenschaften an der Universität Kiel (IFM-GEOMAR), Kiel, Germany.
[3] Leibniz-Institut für Meereswissenschaften an der Universität Kiel (IFM-GEOMAR), Kiel, Germany.

0148-0227/10/2009JC005869

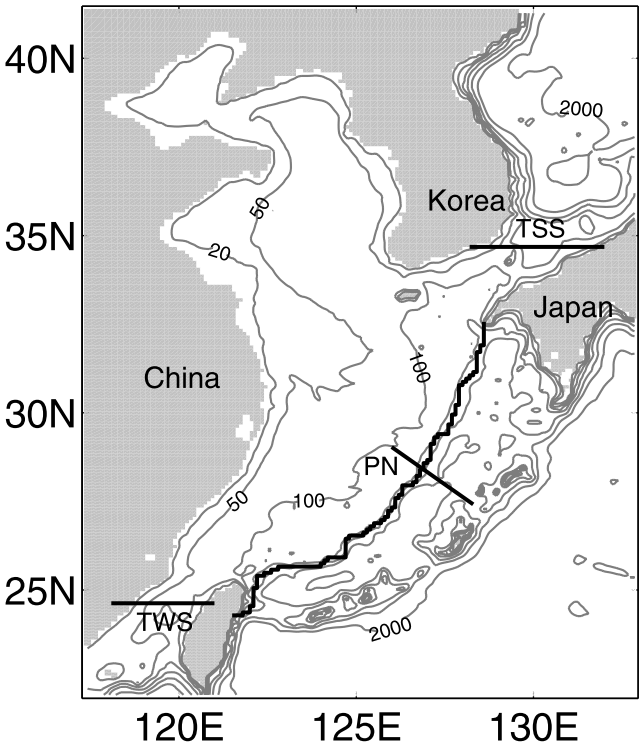

Figure 1. Model bathymetry in the East China Sea (ECS). The contours with numbers are isobaths with units in meters. The position of sections is shown for reference. TWS, Taiwan Strait; TSS, Tsushima Strait; PN, Pollution Nagasaki line. The shelf break (here defined as the 200 m isobath) which roughly coincides with the Kuroshio front is contoured with a thick black line.

observed. So, the modeling should be carried out in a basinwide domain with boundary conditions consistent with observations. Note that a local marginal sea model depends strongly on the artificial boundary conditions along the open boundary, where the structures of the currents as well as their temporal variations are usually unknown. A global ocean model, on the other hand, is able to avoid the problem of open boundary conditions. However, the model has to adequately resolve the steep shelf break in the ECS along which the Kuroshio flows and the ECS itself. Across the shelf break, the water depth varies from 200 m to more than 1000 m over a distance of 20–30 km. This requires the model resolution to be <10 km. The vertical structure of the Kuroshio needs to be resolved because the interaction between topography and baroclinicity is crucial to the cross-front currents in the ECS [*Isobe*, 2000; *Guo et al.*, 2003]. Note that increasing the model's horizontal resolution can also improve the performance of the vertical structure of Kuroshio over the shelf break [*Guo et al.*, 2003]. In this study, a global ocean circulation model with regionally increased horizontal resolution (1/10°) in the ECS was used to satisfy these two requirements. The model is based on the Geophysical Fluid Dynamics Laboratory (GFDL) Modular Ocean Model Version 4 (MOM4) [*Griffies et al.*, 2005].

[5] The article is organized as follows: A description of our numerical model is provided in section 2. Model results and comparison with observations are given in section 3. In section 4, we discuss the temperature flux in the ECS, focusing on the Kuroshio onshore temperature flux across the shelf-break. A discussion on processes driving the Kuroshio onshore temperature flux across the shelf break is given in section 5. Section 6 gives a final summary.

2. Model Configuration

[6] This work is based on integrations of the MOM4p0d (GFDL Modular Ocean Model v.4 [*Griffies et al.*, 2005]) z-coordinate, free surface ocean general circulation model. The model region covers the entire global ocean with an enhanced meridional and zonal resolution in the ECS (Figure 1). Figure 2 illustrates the grid area in the model: The horizontal resolution gradually telescopes from a global 2.0° to 1/10° in the ECS. The vertical grid spacing is chosen with attention given to the model's ability to represent the vertical structure of the Kuroshio over the steep shelf break. For this purpose, we placed a total of 59 levels down to 5500 m, with 16 of these in the upper 220 m. The bottom topography is interpolated from the ETOPO5 dataset, a 5 min gridded elevation data set from the National Geophysical Data Center (www.ngdc.noaa.gov/mgg/global/relief/ETOPO5/). In the ECS, however, we used 1/10° gridded data derived from observations and ocean charts (G. Fang, personal communication). (The main advantage of the latter product

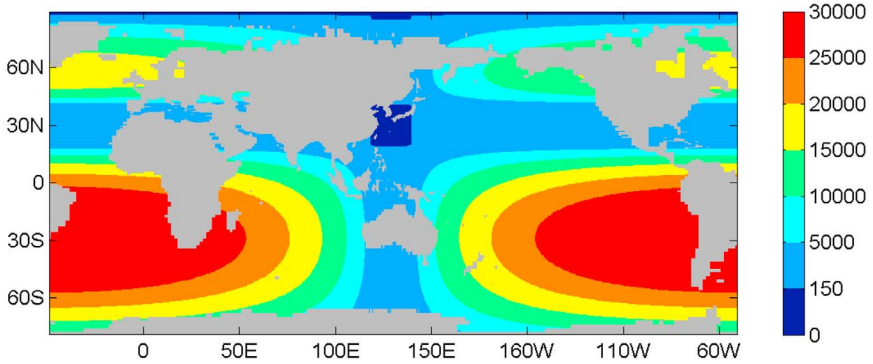

Figure 2. Model horizontal grid area (in km^2). There are a total of 504 zonal grid points and 362 grid points over the latitude range 78°S to 90°N.

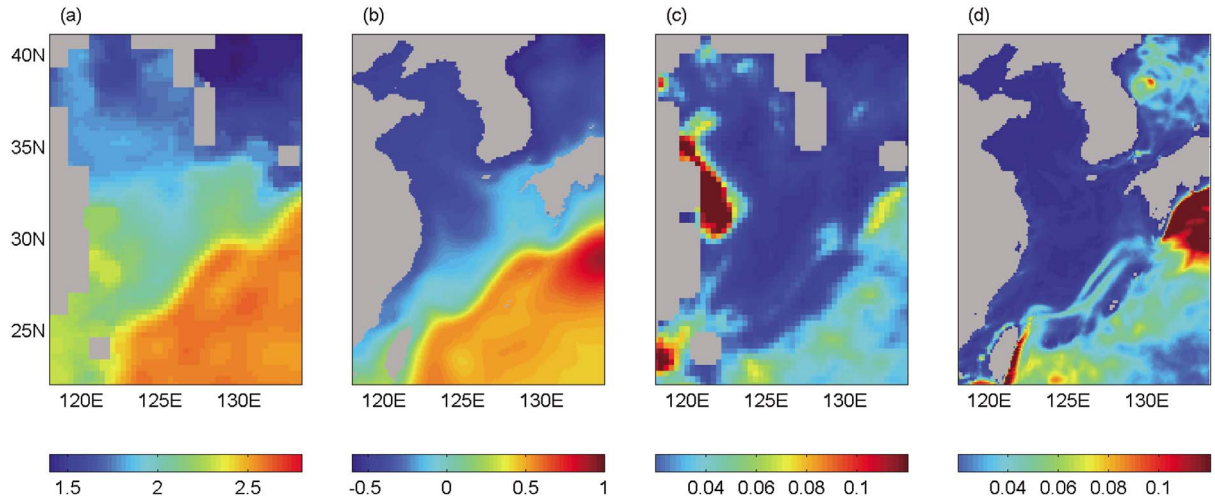

Figure 3. Annual mean sea surface height from (a) satellite altimeter measurements and (b) the model (in meters). Annual mean eddy kinetic energy from (c) satellite altimeter measurements and (d) the model (in m^2/s^2).

over ETOPO5 is an improved representation of the steep shelf break which steers the Kuroshio.)

[7] The atmospheric forcing consists of 6-hourly wind stress, heat, and freshwater flux fields derived from the ERA-40 reanalyses from the European Centre for Medium-Range Weather Forecasts (ECMWF) [*Uppala et al.*, 2005]. In addition to the heat fluxes from ECMWF, a flux correction restores sea surface temperatures (SSTs) with a time scale of 30 days to monthly mean SSTs derived from a blend of satellite products [Rathbone, 2006, personal com-

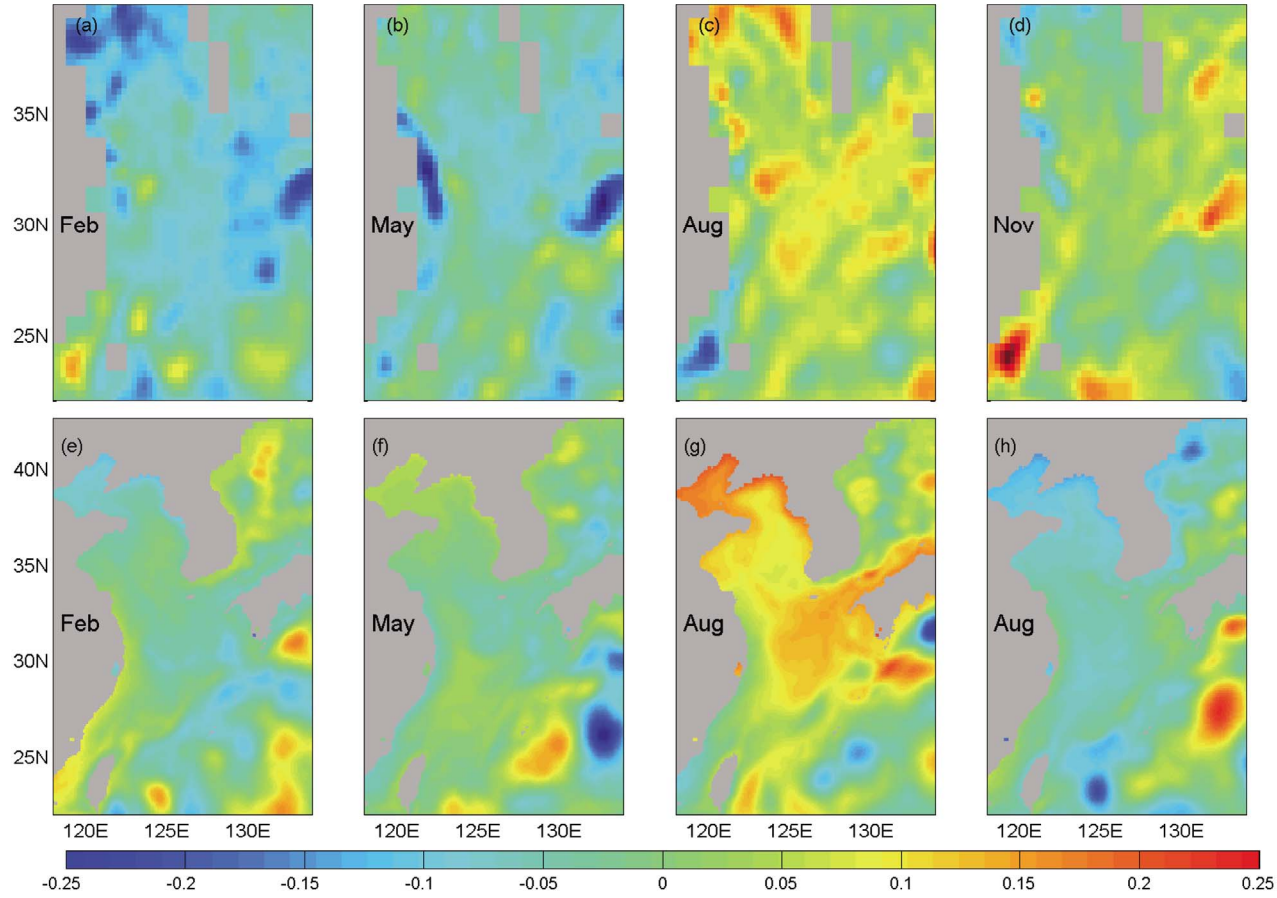

Figure 4. Seasonal anomalies of sea surface height (in meters) from (a–d) satellite altimeter measurements and (e–h) the model in February, May, August, and November.

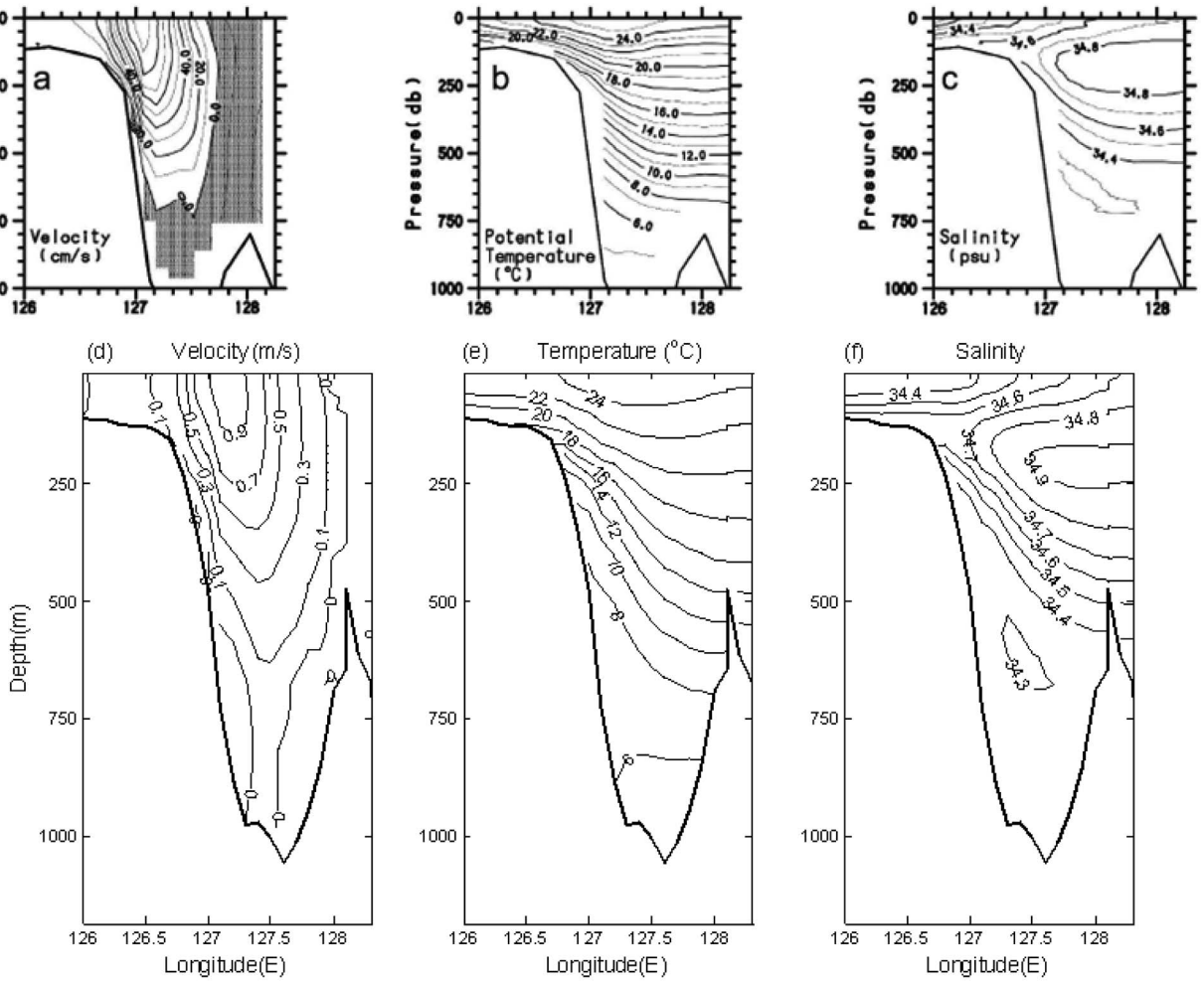

Figure 5. Observed data along the PN line for (a) along-shelf velocity, (b) potential temperature, and (c) salinity [from *Guo et al.*, 2006]. Model results of (d) along-shelf velocity, (e) potential temperature, and (f) salinity.

munication]. The vertical mixing of momentum and scalar tracers is parameterized following the work of *Large et al.* [1994]. In the surface mixed layer, vertical diffusivities and viscosities are derived from a K-profile parameterization (KPP) mixed layer model. The relevant parameters are (1) a critical bulk Richardson number of 0.3 and (2) vertical background diffusivity and viscosity of 10^{-5} m^2 s^{-1}. (Note that the constant background values apply also below the surface mixed layer throughout the water column.) Both parameterizations of the nonlocal and the double diffusive (vertical) scalar tracer fluxes are applied. The integration started from rest with initial temperatures and salinities interpolated from *Conkright and Boyer* [2002]. An analysis of the simulated mean sea surface height indicates that the model reaches a state of quasi-equilibrium in the ECS after 2 years of integration, i.e., the spin-up time of 2 years appears sufficient for the ECS, and we expect not much difference for longer spin-up periods. Note, however, that the large-scale circulation in the Pacific Ocean needs a longer spin-up period to reach quasi-equilibrium. After 2 years of spin-up, the model was integrated for a period of 5 years from 1995–1999. The subsequent calculations are all based on the final 5 year period. In all other respects, not described here, the model configuration is identical to the one described by *Oke et al.* [2005].

3. Model Evaluation

3.1. Sea Surface Height and Eddy Kinetic Energy

[8] The dominant features of the large-scale circulation in the ECS are captured by the mean of the sea surface height in the model and from the JASON and TOPEX/POSEIDON mission's satellite altimeter measurements between 1995 and 1999 (Figures 3a and 3b). The altimeter products have been produced by SSALTO/DUACS and are distributed by AVISO on a 1/3 × 1/3 grid. The sea surface height (SSH) images are generally characterized by a sea surface tilting along the shelf break between Taiwan and Japan. High sea level is situated on the offshore side of the shelf break, and low sea level shows up in the ECS. The seasonal cycle of simulated SSH anomaly (Figure 4) agrees well with the observations in both pattern and amplitudes. A low sea level appears in winter, and a high sea level peak occurs in summer.

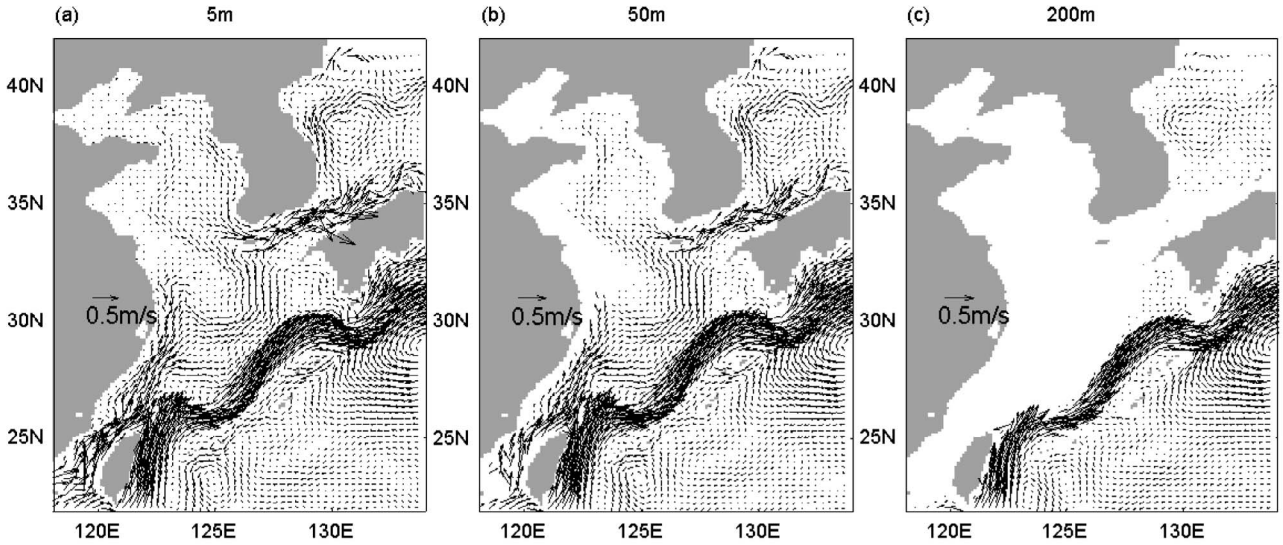

Figure 6. Annual mean velocity distribution in the ECS in (a) the surface layer (5 m), (b) the middle layer (50 m), and (c) the lower layer (200 m).

[9] The surface eddy kinetic energy (EKE) characterizing the mesoscale activity is defined as follows:

$$EKE = \overline{0.5(u'^2 + v'^2)},$$

where u′ and v′ are deviations of the surface horizontal velocities from their time mean, respectively. The 5 year average from 1995 to 1999 shown in Figure 3d for the model can be compared with an estimate derived from observations (Figure 3c). As seen in the observations, the model EKE has a maximum of about 0.07 m^2/s^2 in the area east of the Ryukyu Islands and east of Taiwan. This maximum might be due to the short-term variability of Kuroshio triggered by active mesoscale eddies coalescing with the circulation [*Ichikawa*, 2001; *Zhang et al.*, 2001; *Yang et al.*, 1999]. A weaker maximum is found along the shelf break, where the active mesoscale meandering perturbs the Kuroshio frequently [*Sugimoto et al.*, 1988; *Qiu et al.*, 1990; *Ichikawa and Beardsley*, 1993; *James et al.*, 1999]. The magnitude of the modeled EKE is somewhat higher than the estimate derived from the observed SSH variability along the Kuroshio, to the east of Ryukyu Islands, and in the Japan Sea. However, the larger values are most prominent in the vicinity of the simulated EKE maximum. The larger values of modeled EKE point toward a known low bias in SSH-derived EKE [*Fratantoni*, 2001]. Note that the reverse holds for coastal areas, especially in estuaries and in the Taiwan Strait, where the observations imply a local maximum but the model does not. This, however, is most likely an observational artifact as altimetry observations are biased by tidal signals which are not associated with EKE. Overall, the EKE pattern with a maximum along the Kuroshio and an offshore increase are rather well reproduced by the model.

3.2. Baroclinic Structure of the Along-Shore Kuroshio Current

[10] We compare the model results with observations along the Pollution Nagasaki (PN) line across the Kuroshio to evaluate the modeled vertical structure. The PN line [*Oka and Kawabe*, 1998; http://www.jma-net.go.jp/nagasaki/kaiyo/knowledge/pn/index.html] (see Figure 1 for its position) is a section regularly sampled by the Nagasaki Marine Observatory, and long-term hydrographic data are available. Figure 5 shows the modeled along-shelf velocity, temperature, and salinity fields at the PN line.

[11] The modeled mean volume transport through the PN line is 25.8 Sv, which is consistent with the value of 25.4 Sv calculated from the geostrophic velocity referred to 700 m [*Hinata*, 1996]. Comparison of the model results with the PN line observations and the surface current distributions [*Oka and Kawabe*, 1998; *Oka*, 2000] confirms that there is good agreement between the observed annual mean current (Figure 5a) and the simulated current (Figure 5d) in terms of current strength, location of the strongest current, and horizontal and vertical gradients of the current. Furthermore, there is good agreement between the observed (Figures 5b and 5c) and simulated (Figures 5e and 5f) mean potential water temperature and salinity. We conclude that the model features a good representation of both the circulation in the ECS and the vertical field around the shelf break. The latter, which includes an appropriate representation of the vertical structure of the Kuroshio, is a precondition for modeling reliable cross-isobath intrusion of the Kuroshio in the model.

3.3. Current Distribution in the ECS

[12] The annual mean (1995–1999) velocity at the surface, at 50 m, and at 200 m in the ECS is shown in Figure 6. The Kuroshio at the three levels shows a similar pattern to that observed by *Tang et al.* [2000]: After impinging on the shelf break northeast of Taiwan, the Kuroshio turns northeastward and flows along the shelf break up to the area around 30°N, 129°E, where it turns eastward and then exits the ECS through the Tokara Strait. The strength and width of the modeled Kuroshio are about 1 m/s and 100 km, respectively, which are consistent with observations by *Fang et al.* [1991].

Table 1. List of Season-Averaged and Annual Mean Volume Transport, Temperature Flux, and Freshwater Transport in Each Channel in the East China Sea and Their Standard Deviation From Seasonal Means and the Annual Mean[a]

	Spring	Summer	Autumn	Winter	Annual
			Volume Transport (Sv)		
TWS	2.22 ± 0.16	2.84 ± 0.35	1.34 ± 0.30	1.13 ± 0.37	1.88 ± 0.32
TSS	2.41 ± 0.14	3.05 ± 0.39	3.35 ± 0.32	2.43 ± 0.38	2.81 ± 0.18
Front	0.17 ± 0.22	0.19 ± 0.57	2.05 ± 0.42	1.32 ± 0.52	0.93 ± 0.51
			Temperature Flux (PW)		
TWS	0.23 ± 0.02	0.32 ± 0.02	0.15 ± 0.02	0.11 ± 0.04	0.20 ± 0.03
TSS	0.13 ± 0.01	0.25 ± 0.04	0.30 ± 0.04	0.15 ± 0.03	0.21 ± 0.01
Front	−0.02 ± 0.03	−0.05 ± 0.06	0.17 ± 0.05	0.10 ± 0.05	0.05 ± 0.03
			Freshwater Transport ($\times 10^9$ kg/s)		
TWS	2.20 ± 0.16	2.62 ± 0.20	1.32 ± 0.21	1.12 ± 0.37	1.81 ± 0.31
TSS	2.35 ± 0.13	2.90 ± 0.39	3.20 ± 0.32	2.39 ± 0.37	2.71 ± 0.18
Front	0.11 ± 0.22	0.19 ± 0.56	1.99 ± 0.42	1.26 ± 0.52	0.89 ± 0.48

[a]The first and second numbers inside each box in columns 3–6 are the seasonal mean and standard deviation of seasonal means, respectively. The first and second numbers in the last column are the annual mean and standard deviation of annual mean, respectively. Sv, sverdrups (106 m^3/s); PW, XXXXX; TWS, Taiwan Strait; TSS, Tsushima Strait.

[13] The strong current which flows into the ECS from the Taiwan Strait is referred to as the Taiwan Warm Current (TWC). It flows in a northeastward direction initially but turns eastward around 26°N, 123°E. After flowing farther eastward to 126°E, it turns northeastward following the local bathymetry and finally, with part of the branch of the Kuroshio, enters the TSS. The TWC meets the Kuroshio water north of Taiwan and is clearly reproduced by the model. The Kuroshio branches southwest of the Kyushu (126°E, 32°N) and flows northward. The majority of the northward current flows through the TSS at 5 m and 50 m. After passing the TSS, the western branch of the TSS throughflow flows along the eastern coast of Korea and goes northward to ~37°N, whereas the eastern branch flows along the coast of Japan. At 50 m, the current distribution is quite similar to that at the surface. The Kuroshio intrusion which occurred preferably northeast of Taiwan features a northward current west of Japan with the same strength as in the upper layer. At 200 m, the intrusion of the Kuroshio northeast of Taiwan can still be identified.

[14] The annual mean volume transports across the TWS, the TSS, and the Kuroshio front (see Figure 1 for their locations) are listed in Table 1. The mean volume transport through the Taiwan Strait is 1.88 Sv. This is slightly larger than the value of 1.6 Sv estimated by *Zhao and Fang* [1991] using observational data, and it is close to the value of 1.8 Sv estimated by *Wang et al.* [2003] on the basis of shipboard ADCP data averaged over 2.5 years. The mean volume transport through the TSS is 2.81 Sv, which is close to the value of 2.7 Sv estimated by *Teague et al*. [2002] using the observation data. The averaged onshore cross-frontal volume transport is 0.93 Sv. It is slightly less than the value of 1.4 Sv estimated by *Isobe* [2008] using ADCP observations in TWS and TSS. The difference might be due to interannual variation of the onshore transport. Table 1 gives the seasonal mean and annual mean values and the standard deviations of the annual mean and seasonal means of volume transport, temperature flux, and freshwater transport through the TWS, the TSS, and the 200 m isobath in the ECS. The volume transport is at a minimum in winter and autumn for the TWS and at a maximum in summer. The volume transport across the 200 m isobath is at a maximum in autumn and at a minimum in spring. The standard deviations of the annual mean values for TWS, TSS, and 200 m isobath are 0.32, 0.18, and 0.51 Sv, respectively. Note that disagreement between the model results and previous observational estimates is thus within the bound of interannual variability. The mean volume transport through the TWS in autumn is larger than the value of 0.14 Sv in fall estimated by *Teague et al.* [2003]. It should be noted that the period considered by *Teague et al.* [2003] was limited to October–December 1999, and as such their result does not represent a long-term average. Note that the volume transport estimated by the model is 1.23 Sv in autumn 1999. The value from *Teague et al.* [2003] is much smaller than this. As listed in Table 1, the standard deviation in fall of the volume transport through the TWS is 0.30 Sv. The value of 0.14 Sv estimated by *Teague et al.* [2003] lies outside 2 standard deviations of the modeled seasonal average of 1.23 Sv in autumn 1999. The model-based estimate and the value presented by *Teague et al.* [2003] appear therefore to be inconsistent. In the model, the volume transports through these three sections that enclose the ECS are balanced, i.e., the residual of the volume transport through TWS and TSS is supplied by the onshore flux across the shelf break. Note that the volume transport of Changjiang River entering the ECS is ~0.03 Sv, thus the volume transport due the river runoff, which we do not include in the model, seems negligible.

4. Temperature Flux in the ECS

[15] As the Kuroshio carries an enormous amount of seawater and heat northward, it plays an important role in the ECS. The temperature flux from the Kuroshio to the ECS is a key factor in understanding the heat balance in the ECS. The role of Kuroshio for the ECS is primarily determined by its ability to transport heat shoreward. The

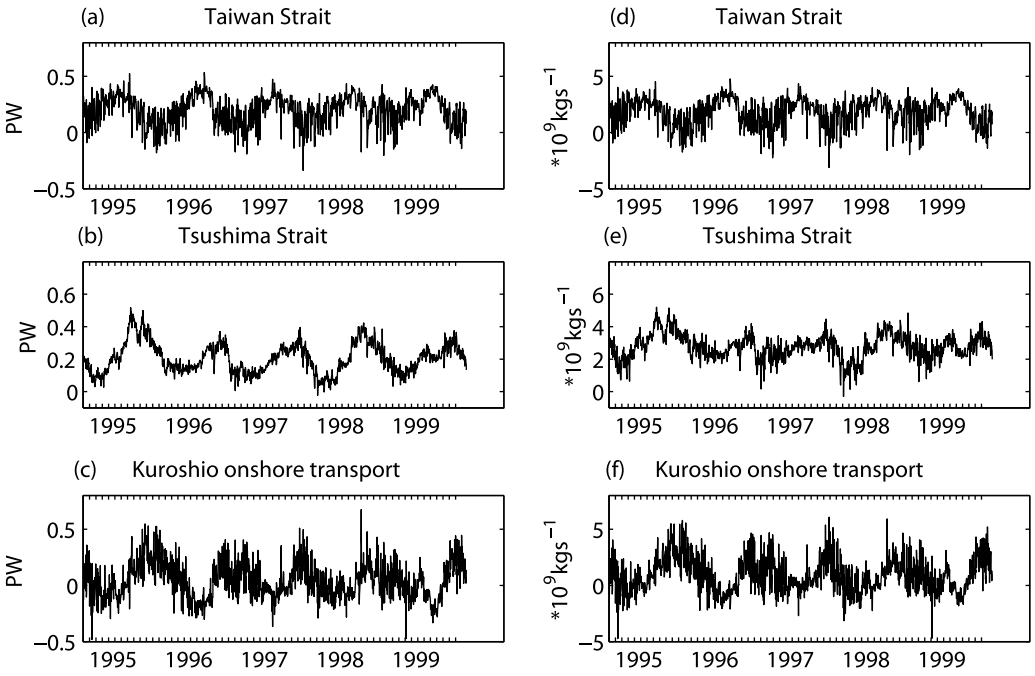

Figure 7. Time series of (a–c) daily temperature flux and (d–f) freshwater transport through Taiwan Strait (Figures 7a and 7d), Tsushima Strait (Figures 7b and 7e), and 200 m isobath (Figures 7c and 7f).

oceanic temperature flux across a given section is defined as follows:

$$Q = \iint \rho c_p \theta u dx dz, \tag{1}$$

where ρ is the seawater density, c_p is the specific heat capacity of seawater at constant pressure, θ is the potential temperature (measured here in °C); and u, the current velocity perpendicular to the section. The coordinates x and z are set along the selected section and the vertical direction, respectively. In the present study, ρc_p is assumed to be constant, i.e., $\rho c_p = 4.28 \times 10^6$ JK^{-1} m^{-3}. Note that for $\int\int udxdz = 0$, the temperature flux Q becomes a heat flux.

[16] The water exchange in the ECS takes place in the main channels, which are TWS, the TSS, and the 200 m isobath connecting Taiwan and Japan. The cross-isobath water exchange is reduced by the frontal meandering along the shelf break. Heat transported by the current goes in or out the ECS through these sections. Similar to the heat flux, the freshwater transported by the ocean is defined as, $F = \int\int \rho u(1 - S)dxdz$ where S is the (dimensionless) salinity of seawater [*Wijffels et al.*, 1992]. The time series of temperature flux and freshwater transport through these sections are shown in Figure 7. The averaged temperature fluxes across all selected sections in the ECS are listed in Table 1. The time-averaged temperature flux through TWS, TSS, and the 200 m isobath are 0.20 PW, 0.21 PW, and 0.05 PW, respectively. The residual heat flux of three channels is balanced by the surface heat loss of 0.035 PW in the ECS. The surface heat loss averaged over the ECS is calculated from the net surface heat flux (−45 W/m^2) derived from the ECMWF dataset multiplying the area of the ECS (7.7×10^{11}m^2), i.e., 0.035 PW. The interannual standard deviation of temperature flux through TWS, TSS, and the 200 m isobath are 0.03 PW, 0.01 PW, and 0.03 PW, respectively. The difference between the model result and previous observational estimations might be related to the uncertainties due to interannual variability.

[17] In the ECS, the seasonal cycle of freshwater transport through each channel is similar to that of the temperature flux. From September to October, the Kuroshio onshore freshwater transport reaches its maximum of about 3.4×10^9 kg/s, and then it begins to decrease gradually. The time-averaged freshwater transport through TWS, TSS, and the 200 m isobath are 1.81×10^9 kg/s, 2.71×10^9 kg/s, and 0.89×10^9 kg/s, respectively. We found that a net freshwater transported 0.01×10^9 kg/s out the ECS. This is larger than the estimate of transport of 0.002×10^9 kg/s into the ECS by *Fang et al.* [2003] using a global ocean model. The interannual standard deviations of freshwater transport through TWS, TSS, and the 200 m isobath are 0.31×10^9 kg/s, 0.18×10^9 kg/s, and 0.48×10^9 kg/s, respectively.

[18] The seasonal variation of temperature flux in the TWS is significant with a maximum (~0.33 PW) in July and a minimum (~0.10 PW) in December. This is consistent with the variability of volume transport on the basis of current metric data reported by *Fang et al.* [1991]. The time series of Kuroshio onshore flux across the 200 m isobath has the most significant signal in seasonal variability. From September to October, the Kuroshio onshore flux reaches its maximum of about 0.19 PW, and then it begins to decrease gradually until reaching its minimum from June to July. In addition to the seasonal variability, short-term variations are also prominent in the time series of the daily Kuroshio onshore flux across the 200 m isobath.

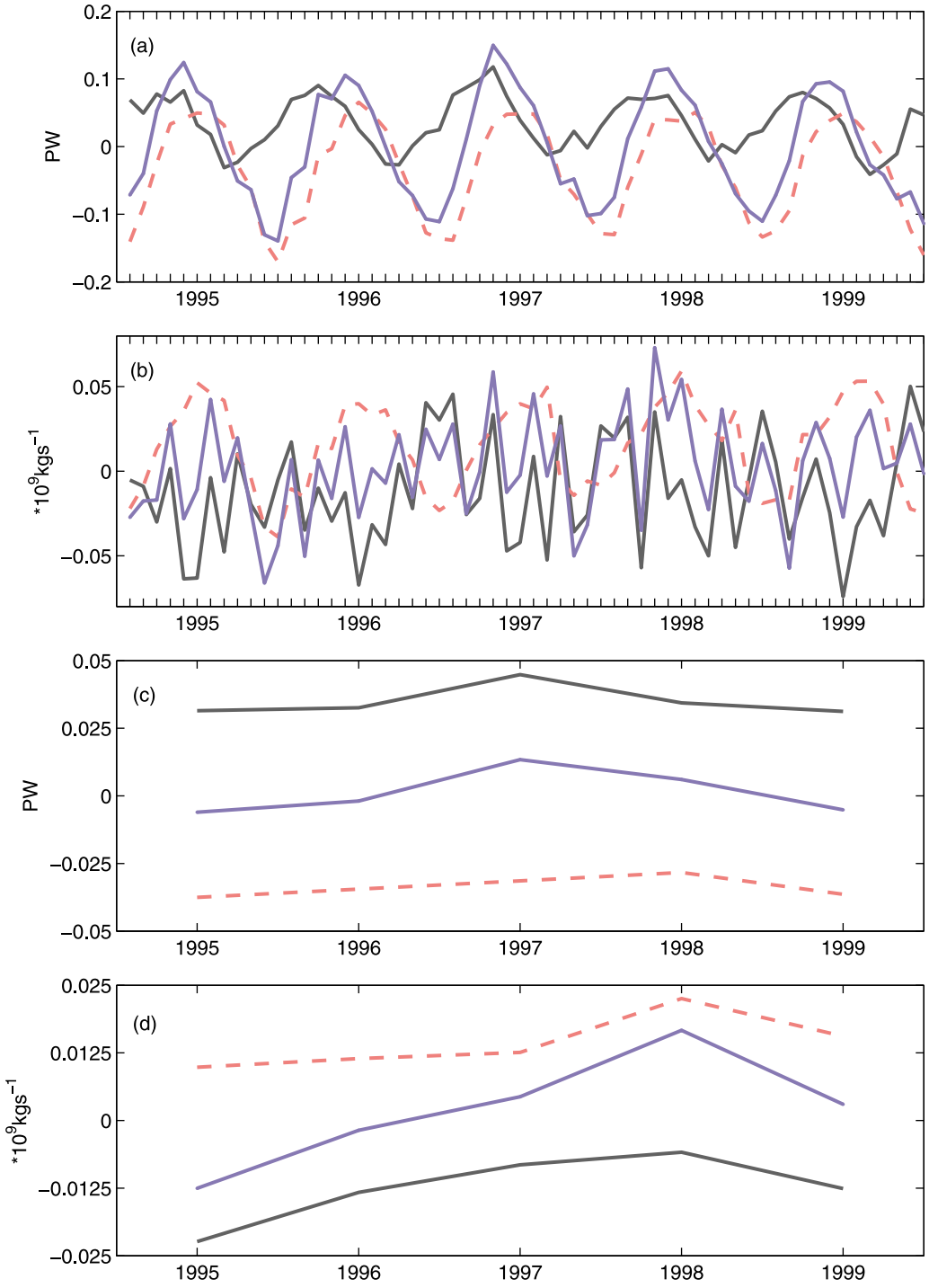

Figure 8. Seasonal variations of (a) heat budget (in PW), (b) freshwater budget (in kg/s) in the ECS. Interannual variations in (c) heat budget (in PW) and (d) freshwater budget (in kg/s) in the ECS. In Figures 8a and 8c, residual heat flux of three channels is denoted by a black line, and surface heat flux spatially averaged over the ECS is denoted by a red dashed line, and heat storage is denoted by blue line. In Figures 8b and 8d, residual freshwater transport of three channels is denoted by a black line, surface freshwater flux (including river runoff) spatially averaged over the ECS is denoted by a red dashed line, and freshwater storage is denoted by a blue line.

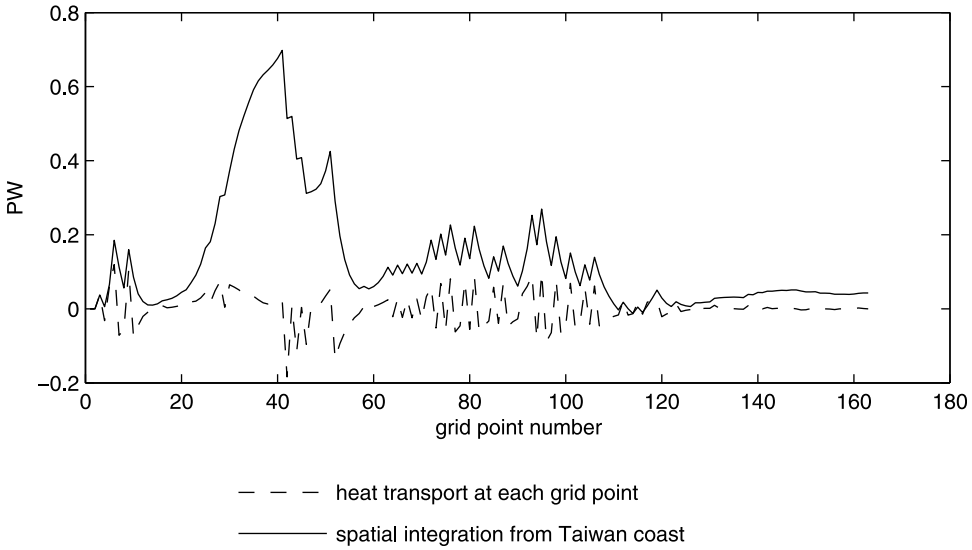

Figure 9. Time-averaged Kuroshio onshore temperature flux at each grid point of the 200 m isobath. Its spatial integration from Taiwan coast to a given grid point of the 200 m isobath (in PW).

[19] Figure 7 shows that short-term variations are prominent in the variations of the Kuoshio onshore heat flux. To study the contribution of short-term variations in the temperature flux, the effect of eddy-induced temperature flux is discussed. The velocity and temperature can be subdivided by using the following definition:

$$u = \overline{u} + u'; \overline{u} = [\overline{u}] + \overline{u}^*; \qquad \theta = \overline{\theta} + \theta'; \overline{\theta} = [\overline{\theta}] + \overline{\theta}^*; \tag{2}$$

where the overbar and prime represent a local time average and an instantaneous departure from that average and the brackets and asterisk represent an average along the shelf break and a local departure from that average

$$[\overline{u\theta}] = [\overline{u}][\overline{\theta}] + [\overline{u'\theta'}] + \left[\overline{u}^*\overline{\theta}^*\right].$$

[20] The first right-hand term gives the mean temperature flux. The second right-hand term, which represents the space mean of local eddy flux, is called the transient eddy temperature flux. This is the average over space of the eddy flux at individual grid points due to the correlation in time of u and θ. It can be considered to be the onshore heat transported by transient eddies. The third right-hand term represents the standing eddy temperature flux. It results from the correlation in space between the time mean of u and θ over a given period of time.

[21] The time-mean total temperature fluxes, as well as the transient and standing eddy transport across the 200 m isobath, are calculated and listed in Table 1. The onshore temperature flux for the ECS is approximately 0.05 PW. The transient eddy temperature flux across the 200 m isobath is 0.005 PW and contributes 11.2% to the total temperature flux. The standing eddy temperature flux is 0.013 PW and gives 27.1% to the total temperature flux. The remainder of the temperature flux is supplied by the mean temperature flux. The large meander northeast of Taiwan contributes largest to the onshore stranding eddy temperature flux. The mean temperature flux contributes ~61.7% to the total temperature flux.

[22] To examine the seasonal and interannual variability of each term of heat and freshwater budget, the monthly mean and annual mean of residual transport, surface flux, and storage of heat and freshwater are plotted in Figure 8. The spatially averaged surface heat and freshwater flux are derived from the ECMWF dataset forcing the model, in which the river runoff is included in the freshwater flux. In Figure 8a, on seasonal time scales, the variations of heat storage are determined by the surface heat flux, whereas on interannual time scales, it is determined by the residual heat flux of three channels. On seasonal time scales, the variations of freshwater storage are determined by the residual transport of three channels, whereas on interannual time scales, it is determined by the surface freshwater flux.

5. Discussion

[23] The spatial distribution of the time-averaged temperature flux across the 200 m isobath (Figure 9) shows that the Kuroshio intrusion northeast of Taiwan is the major source of the mean Kuroshio onshore flux to the ECS. This is seen more clearly in the spatially integrated onshore flux starting from the coast of Taiwan. The first 60 grid points (i.e., the line 121.5°E, 24.3°N, to 124.8°E, 26.5°N) and the grid point 120 to 160 (i.e., the line 127.6°E, 29.4°N, to 128.6°E, 32.2°N) are the two major locations on the 200 m isobath providing the onshore temperature flux. The temperature flux through the first 60 grids is 0.07 PW, and the section of grid point 120 to 160 provides 0.01 PW. Approximately 0.03 PW is transported offshore between the grid points 60 to 120.

[24] To understand the dynamics for the seasonality of the Kuroshio onshore temperature flux, we refer to the wind stress and the wind-induced Ekman transport. In winter, the wind stress over the ECS is characterized by strong winds from the north, associated with the East Asian monsoon. During summer, southerly winds prevail over northerly winds, and the wind stress appears to be connected with the

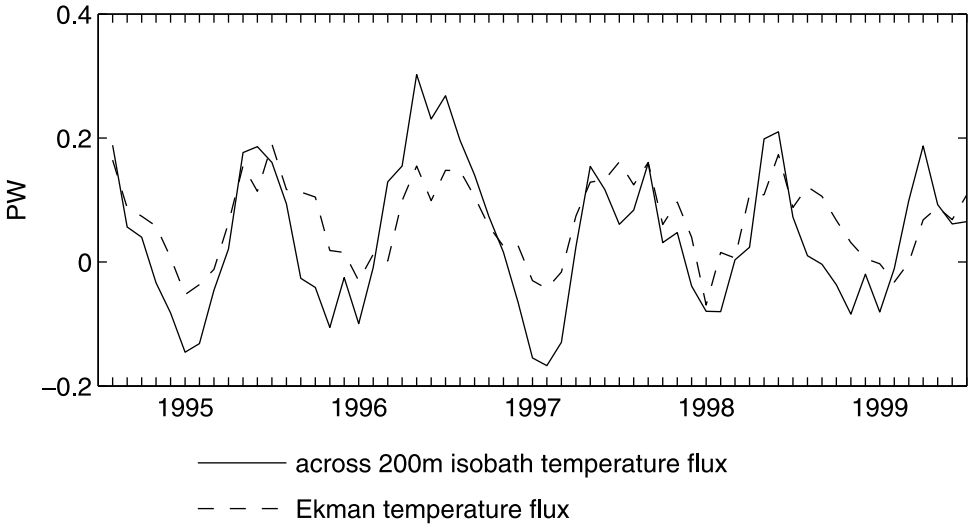

Figure 10. Monthly Kuroshio onshore temperature flux across the 200 m isobath and monthly Ekman temperature flux across the 200 m isobath.

corresponding southerly summer monsoon. The Ekman temperature flux across the 200 m isobath is a part of the total Kuroshio onshore flux in the ECS, and its seasonal variation is generally in phase with the Kuroshio onshore flux (Figure 10). The Ekman temperature flux is defined as

$$Q_E = \int \rho c_p \theta_s \left(-\frac{\tau_x}{f\rho} + \frac{\tau_y}{f\rho} \right) dx,$$

where $(-\frac{\tau_x}{f\rho}, -\frac{\tau_y}{f\rho})$ is the Ekman volume transport and θ_s is the sea surface temperature. The difference between them reaches a minimum in March, increases gradually from March to September, peaks at a maximum in October, and decreases from November to March. As part of the total Kuroshio onshore flux, the Ekman transport is a major contributor to the seasonal variations of onshore across front temperature flux.

6. Summary

[25] We estimated the oceanic heat and freshwater transport in the ECS using a global ocean model with a regionally refined horizontal grid. The modeled sea surface height variability and eddy kinetic energy are consistent with those derived from satellite altimetry. We found significant levels of EKE east of the Ryukyu Islands and east of Taiwan, where the short-term variability is spawned by active mesoscale eddies coalescing with the circulation. The simulated cross-shore vertical structure of the Kuroshio along the PN line and the volume transport through each channel and the 200 m isobath in the ECS were in good agreement with previous observational estimates [*Oka and Kawabe*, 1998; *Zhao and Fang*, 1991; *Teague et al.*, 2002, 2003; *Isobe*, 2008]. This enhances our confidence in the model-derived heat and freshwater transport estimates presented here.

[26] On basis of the final 5 year period after 2 years of spin-up, the time-averaged temperature flux across TWS, TSS, and the 200 m isobath are 0.20 PW, 0.21 PW, and 0.05 PW, respectively. The residual heat flux into the ECS is 0.04 PW, which is balanced by the surface heat flux. Together with the surface heat flux, the temperature flux through three channels forms the heating system in the ECS. The time-averaged freshwater transport through TWS, TSS, and the 200 m isobath are 1.81×10^9 kg/s, 2.71×10^9 kg/s, and 0.89×10^9 kg/s, respectively, and a net freshwater of 0.01×10^9 kg/s is transported out of the ECS. The eddy temperature flux across the 200 m isobath is 0.005 PW, which accounts for 11.2% of the total temperature flux. The Kuroshio onshore temperature flux happens preferably east of Taiwan and shows a strong seasonal variation with a maximum in autumn and a minimum in summer. The Ekman temperature flux induced by the wind stress in the ECS shows the same seasonal cycle and amplitude with the onshore temperature flux. So, we conclude that the Ekman temperature flux dominates the seasonal cycle of the Kuroshio onshore flux.

[27] **Acknowledgments.** N. Liu was supported by the China Scholarship Council. This study was supported by the National Basic Research Program of China grants 2007CB481804 and 2005CB422303, the International Science and Technology Cooperation Program of China grant 2006DFB21250, the Natural Science Foundation of China grants 40706006 and 40930844, the Ministry of Education's 111 Project grant B07036, and the Program for New Century Excellent Talents in University grant NECT-07-0781.

References

Conkright, M. E., and T. P. Boyer (2002), World Ocean Atlas 2001: Objective Analyses, Data Statistics, and Figures, CD-ROM documentation, 17 pp., Natl. Oceanogr. Data Cent., Silver Spring, Md.

Fang, G., B. Zhao, and Y. Zhu (1991), Water volume transport through the Taiwan Strait and the continental shelf of the East China Sea measured with current meters, in *Oceanography of Asian Marginal Seas*, edited by K. Takano, pp. 345–358, Elsevier, New York.

Fang, G., Z. Wei, B.-H. Choi, K. Wang, Y. Fang, and W. Li (2003), Inter-basin freshwater, heat and salt transport through the boundaries of the East and South China Seas from a variable-grid global ocean circulation model, *Sci. China Ser. D Earth Sci.*, *46*(2), 149–161.

Fratantoni, D. M. (2001), North Atlantic surface circulation during the 1990's observed with satellite-tracked drifters, *J. Geophys. Res.*, *106* (C10), 22,067–22,093, doi:10.1029/2000JC000730.

Griffies, S. M., M. J. Harrison, R. C. Pacanowski, and A. Rosati (2005), *A Technical Guide to MOM4*, Geophysical Fluid Dynamics Laboratory, NOAA, Princeton, N. J.

Guo, X., H. Hukuda, Y. Miyazawa, and T. Yamagata (2003), A triply nested ocean model for simulating the Kuroshio: Roles of horizontal resolution on JEBAR, *J. Phys. Oceanogr.*, *33*, 146–169.

Guo, X., Y. Miyazawa, and T. Yamagata (2006), The Kuroshio onshore intrusion along the shelf break of the East China Sea: The origin of the Tsushima Warm Current, *J. Phys. Oceanogr.*, *36*, 2205–2231.

Hinata, T. (1996), Seasonal variation and long-term trends of the oceanographic conditions along a fixed hydrographic line crossing the Kuroshio in the East China Sea, *Oceanogr. Mag.*, *45*, 9–32.

Ichikawa, H., and R. C. Beardsley (1993), Temporal and spatial variability of volume transport of the Kuroshio in the East China Sea, *Deep Sea Res.*, *40*, 583– 605.

Ichikawa, K. (2001), Variation of the Kuroshio in the Tokara Strait induced by meso-scale eddies, *J. Oceanogr.*, *57*, 55–68.

Isobe, A. (2000), Two-layer model on the branching of the Kuroshio southwest of Kyushu, Japan, *J. Phys. Oceanogr.*, *30*, 2461–2476.

Isobe, A. (2008), Recent advances in ocean-circulation research on the Yellow Sea and East China Sea shelves, *J. Oceanogr.*, *64*, 569–584.

Isobe, A., and R. C. Beardsley (2006), An estimate of the cross-frontal transport at the shelf break of the East China Sea with the Finite Volume Coastal Ocean Model, *J. Geophys. Res.*, *111*, C03012, doi:10.1029/2005JC003290.

Isobe, A., M. Ando, T. Watanabe, T. Senjyu, S. Sugihara, and A. Manda (2002), Freshwater and temperature transports through the Tsushima-Korea Straits, *J. Geophys. Res.*, *107*(C7), 3065, doi:10.1029/2000JC000702.

James, C., M. Wimbush, and H. Ichikawa (1999), Kuroshio meanders in the East China Sea, *J. Phys. Oceanogr.*, *29*, 259–272.

Large, W. G., J. C. McWilliams, and S. C. Doney (1994), Oceanic vertical mixing: A review and a model with nonlocal boundary layer parameterization, *Rev. Geophys.*, *32*(4), 363–403, doi:10.1029/94RG01872.

Lee, J.-S., and T. Matsuno (2007), Intrusion of Kuroshio water onto the continental shelf of the East China Sea, *J. Oceanogr.*, *63*, 309–325.

Matsuno, T., J.-S. Lee, and S. Yanao (2009), The Kuroshio exchange with the South and East China Seas, *Ocean Sci.*, *5*, 303–312.

Oka, E. (2000), Characteristics of variations of water and dynamic properties of the Kuroshio in the East China Sea, Ph.D. thesis, 107 pp., Univ. of Tokyo, Tokyo.

Oka, E., and M. Kawabe (1998), Characteristics of variations of water properties and density structure around the Kuroshio in the East China Sea, *J. Oceanogr.*, *54*, 605–617.

Oke, P. R., A. Schiller, D. A. Griffin, and G. B. Brassington (2005), Ensemble data assimilation for an eddy-resolving ocean model of the Australian region, *Q. J. R. Meteorol. Soc.*, *131*, 3301–3311.

Qiu, B., T. Toda, and N. Imasato (1990), On Kuroshio front fluctuations in the East China Sea using satellite and in situ observational data, *J. Geophys. Res.*, *95*(C10), 18,191– 18,204, doi:10.1029/JC095iC10p18191.

Sugimoto, T., S. Kimura, and K. Miyaji (1988), Meander of the Kuroshio front and current variability in the East China Sea, *J. Oceanogr. Soc. Jpn.*, *44*, 125–135.

Tang, T. Y., J. H. Tai, and Y. J. Yang (2000), The flow pattern north of Taiwan and the migration of the Kuroshio, *Cont. Shelf Res.*, *20*, 349–371.

Teague, W. J., G. A. Jacobs, H. T. Perkins, J. W. Book, K.-I. Chang, and M.-S. Suk (2002), Low-frequency current observation in the Korea/Tsushima Strait, *J. Phys. Oceanogr.*, *32*, 1621–1641.

Teague, W. J., G. A. Jacobs, D. S. Ko, T. Y. Tang, K.-I. Chang, and M.-S. Suk (2003), Connectivity of the Taiwan, Cheju, and Korea straits, *Cont. Shelf Res.*, *23*, 63–77.

Uppala, S. M., et al. (2005), The ERA-40 re-analysis, *Q. J. R. Meteorol. Soc.*, *131*, 2961–3012.

Wang, Y. H., S. Jan, and D. P. Wang (2003), Transports and tidal current estimates in the Taiwan Strait from shipboard ADCP observations (1999–2001), *Estuarine Coastal Shelf Sci.*, *57*, 193–199.

Wijffels, S. E., R. W. Schmitt, H. L. Bryden, and A. Stigebrandt (1992), Transport of fresh-water by the oceans, *J. Phys. Oceanogr.*, *22*, 155–162.

Yang, Y., C.-T. Liu, J.-H. Hu, and M. Koga (1999), Taiwan current (Kuroshio) and impinging eddies, *J. Oceanogr.*, *55*, 609–617.

Zhang, D., T. N. Lee, W. E. Johns, C.-T. Liu, and R. Zantopp (2001), The Kuroshio east of Taiwan: Modes of variability and relationship to interior ocean mesoscale eddies, *J. Phys. Oceanogr.*, *31*, 1054–1074.

Zhao, B.-R., and G.-H. Fang (1991), The estimate of transport of the main water route in the East China Sea, *Acta Oceanol. Sin.*, *13*, 169–178.

H. Dietze, C. Eden, and N. Liu, Leibniz-Institut für Meereswissenschaften an der Universität Kiel (IFM-GEOMAR), D-24105 Kiel, Germany. (nliu@ifm-geomar.de)

X. Lin and D. Wu, Physical Oceanography Laboratory, Ocean University of China, Qingdao, 266100, China.